Title	Pathological processes in aqueous humor due to iris atrophy predispose to early corneal graft failure in humans and mice
Author(s) Alternative	Yamaguchi, T; Higa, K; Yagi-Yaguchi, Y; Ueda, K; Noma, H; Shibata, S; Nagai, T; Tomida, D; Yasu-Mimura, R; Ibrahim, O; Matoba, R; Tsubota, K; Hamrah, P; Yamada, J; Kanekura, K; Shimazaki, J
Journal	Science advances, 6(20): -
URL	http://hdl.handle.net/10130/5237
Right	This is an open-access article distributed under the terms of the Creative Commons Attribution-NonCommercial license, which permits use, distribution, and reproduction in any medium, so long as the resultant use is not for commercial advantage and provided the original work is properly cited.
Description	

HEALTH AND MEDICINE

Pathological processes in aqueous humor due to iris atrophy predispose to early corneal graft failure in humans and mice

Takefumi Yamaguchi[1,2]*, Kazunari Higa[1,2], Yukari Yagi-Yaguchi[1,2], Koji Ueda[3], Hisashi Noma[4], Shinsuke Shibata[5], Toshihiro Nagai[5], Daisuke Tomida[1], Ririko Yasu-Mimura[1,2], Osama Ibrahim[1,2], Ryo Matoba[6], Kazuo Tsubota[1,2], Pedram Hamrah[7,8], Jun Yamada[9], Kohsuke Kanekura[10]*, Jun Shimazaki[1,2]

Corneal endothelial cell (CEnC) loss after corneal transplantation is the major cause of graft failure and remains a clinically relevant challenge to overcome. Accumulated knowledge derived from long-term clinical outcomes suggested that elevated protein levels in the aqueous humor are associated with CEnC loss. However, the full spectrum of driver proteins and molecular processes remains to be determined. Here, we defined the somatic microenvironmental landscape and cellular response across human aqueous humor in samples with poor corneal transplantation clinical outcomes using multiomics analyses and clarified specific driver alterations, including complement activation and disturbed energy homeostasis. These driver alterations were also confirmed in aqueous humor from a novel murine model that spontaneously develops iris atrophy, leading to CEnC loss. The application of the integrative multiomics performed in human samples to the novel murine model will help the development of therapeutic modalities for patients with CEnC loss after corneal transplantation.

INTRODUCTION

Corneal endothelial cells (CEnCs) form a monolayer of hexagonal cells located in the posterior surface of the cornea. CEnCs have a pump/barrier function and maintain corneal transparency. They are arrested in a postmitotic state and have a minimal proliferative capacity in vivo (*1*). CEnCs have a unique property, compensating for cell loss by cell enlargement and migration instead of proliferation and wound healing (*2*). In the human cornea, corneal endothelial cell density (CECD) never increases but rather decreases with age at a rate of 0.5% per year (*3*). This reduction is exacerbated to a rate of 2.6 to 7.8% under pathological conditions, leading to CEnC dysfunction and development of bullous keratopathy (*4*). CEnC dysfunction is the leading cause of corneal transplantation, occupying for 39% of all corneal transplantation cases in the United States and accounting for 180,000 patients per year worldwide. Graft survival rate in low-risk eye conditions, such as keratoconus, exceeds 90% at 10 years after transplantation. In contrast, corneal transplantation graft survival for bullous keratopathy treatment is approximately 30 to 55% at 5 years and less than 20 to 40% at 10 years (*5*). Corneal endothelial decompensation due to postoperative CEnC loss is the primary cause of graft failure (29 to 49%), followed by graft rejection (21 to 27%) (*6*). Thus, CEnC loss after corneal transplantation remains one of the most important clinical challenges to be addressed by ophthalmologists.

CECD decrease rates differ among patients, with some exhibiting rapid CECD decrease after corneal transplantation. Recently, we noticed a rapid postoperative CECD decrease in patient's eyes with severe preexisting iris atrophy after corneal transplantation, whereas patients with a healthy iris showed minimal decrease in CECD (*7*). This suggests that the fate of CECD is, to an extent, already determined by the preoperative condition of the patient's iris. Furthermore, congenital eye diseases harboring pathologic iris conditions, such as Axenfeld-Rieger (A-R) syndrome, or acquired pathologic iris conditions, such as iris cyst, iridoschisis, postsurgical iris atrophy, or iridocorneal endothelium (ICE) syndrome, have accelerated CEnC loss (*8*), often develop corneal endothelial dysfunction clinically (Fig. 1, A and B), and are known to have poor prognosis of transplanted grafts in patients who undergo corneal transplantation due to a rapid decrease in CEnCs (fig. S1, A and B). However, to date, the precise mechanisms underlying the rapid CECD decrease still remain elusive. Anatomically, the aqueous humor (AqH) presents between CEnC and the iris. We hypothesized that iris atrophy coincides with serious pathological alterations in the AqH, leading to CEnC loss in a specific biological pathway. We sought to test our hypothesis and identify the biological processes that drive CEnC loss in actual patients through the use of multiomic strategies from patient-derived samples. By doing so, we found abnormal activation of immune responses and disturbed energy homeostasis at the transcriptome and proteome levels. Furthermore, we confirmed the direct connection among CEnCs, iris, and AqH in a mouse strain that spontaneously develops iris atrophy, mimicking human pathologic iris atrophy. The multiomics landscape of AqH from patients with pathological

[1]Department of Ophthalmology, Tokyo Dental College Ichikawa General Hospital, 5-11-13 Sugano, Ichikawa-shi, Chiba 272-8513, Japan. [2]Department of Ophthalmology, Keio University School of Medicine, 35 Shinanomachi, Shinjuku-ku, Tokyo 160-8582, Japan. [3]Project for Realization of Personalized Cancer Medicine, Cancer Precision Medicine Center, Japanese Foundation for Cancer Research, 3-8-31, Ariake, Koto-ku, Tokyo 135-8550, Japan. [4]Department of Data Science, The Institute of Statistical Mathematics, 10-3, Midori-cho, Tachikawa, Tokyo 190-0014, Japan. [5]Electron Microscope Laboratory, Keio University School of Medicine, 35 Shinanomachi, Shinjuku-ku, Tokyo, Japan. [6]DNA Chip Research Inc., Suzue Baydium 5F, 1-15-1, Kaigan, Minato-ku, Tokyo 105-0022, Japan. [7]Center for Translational Ocular Immunology, Tufts Medical Center, Tufts University School of Medicine, Tufts University, 800 Washington St., Boston, MA 02111, USA. [8]Department of Ophthalmology, Tufts Medical Center, Tufts University School of Medicine, Tufts University, 800 Washington St., Boston, MA 02111, USA. [9]Department of Ophthalmology, Meiji University of Integrative Medicine, Hinotani 6-1, Honoda, Hiyoshi-cho, Nantan-shi, Kyoto 629-0392, Japan. [10]Department of Molecular Pathology, Tokyo Medical University, 6-1-1, Shinjuku, Shinjuku-ku, Tokyo 160-8402, Japan.
*Corresponding author. Email: tym.i.eye.i@gmail.com (T.Y.); Kanekura@tokyo-med.ac.jp (K.K.)

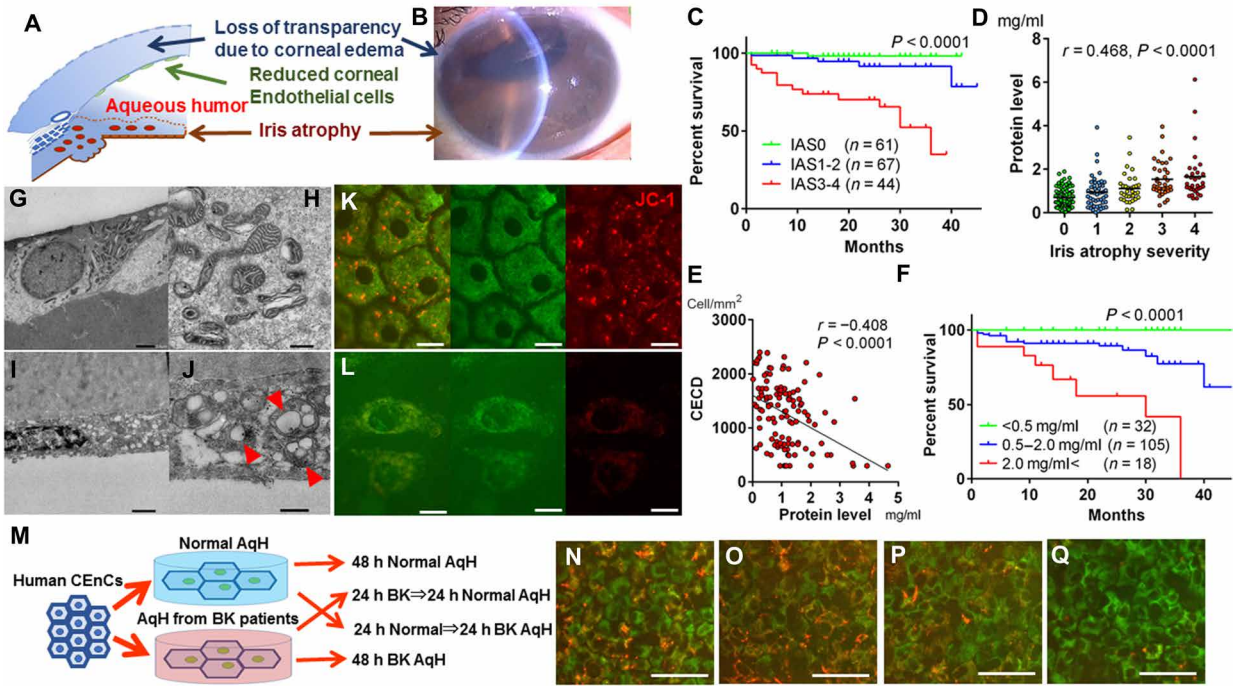

Fig. 1. Condition of iris and AqH determines the prognosis of corneal transplantation. (**A**) CEnCs form a monolayer tissue in the posterior surface of the cornea and play a pivotal role in maintaining corneal transparency. Decreased CEnC number causes irreversible corneal edema, leading to loss of transparency. (**B**) Slit-lamp anterior segment microscopy imaging in A-R syndrome. Loss of transparency due to endothelial dysfunction–induced corneal edema. Pupil is distorted due to iris atrophy. In these eyes, aqueous humor (AqH) is inflamed. Photo credit: Takefumi Yamaguchi, Tokyo Dental College Ichikawa General Hospital. (**C**) Long-term graft survival stratified by iris atrophy severity after endothelial keratoplasty. The prognosis of eyes with severe iris atrophy score (IAS3 to IAS4) was significantly poor (n = 172; log-rank Mantel-Cox test, $P < 0.0001$). (**D**) Protein levels in AqH increase with iris atrophy severity in human eyes (Spearman's correlation analysis, $r = 0.468$, $P < 0.0001$). (**E**) Correlation between preoperative protein levels in AqH and the CECD at 12 months after endothelial keratoplasty (Spearman's correlation analysis, $r = -0.408$, $P < 0.0001$). Other time points are given in table S2. (**F**) Graft survival was significantly shortened in eyes with high preoperative AqH protein levels compared to those with lower protein levels (log-rank Mantel-Cox test, $P < 0.0001$). (**G** to **J**) Representative transmission electron microscopy (TEM) of healthy CEnCs (G and H) and CEnCs of bullous keratopathy (I and J). In bullous keratopathy (I and J), TEM reveals mitochondrial vacuolization, electron-dense deposits, and loss of cristae (red arrowheads). (**K** and **L**) JC-1 staining representing mitochondrial membrane potential in healthy CEnCs (K) and CEnCs of bullous keratopathy (L). Scale bars, 20 μm. (All samples depicted are human). (**M**) Human CEnCs were cultured either in normal AqH cocktail (protein level, 0.466 mg/ml) or AqH cocktail from bullous keratopathy (2.40 mg/ml) for 48 or 24 hours, respectively. (**N** to **Q**) JC-1 staining. CEnCs were cultured in normal AqH for 48 hours (N), in normal AqH cocktail for 24 hours, and then transferred into AqH cocktail from bullous keratopathy for 24 hours (O), vice versa (P), and in AqH cocktail from bullous keratopathy for 48 hours (Q). Scale bars, 50 μm.

CECD decrease will not only help us develop therapeutic modalities for corneal transplantation patients with dysfunctional grafts but also decode the pathological networking among CEnCs, iris, and AqH.

RESULTS

Protein levels in AqH are associated with iris atrophy and poor corneal graft survival

Recent studies have a proposed potential pathophysiological association among the iris, AqH, and CEnCs (*7*–*11*). Because of the minimal proliferative capacity of cells inside the eye, the wound healing process of the iris or CEnCs once damaged is limited. Thus, we hypothesized that iris atrophy can directly cause an irreversible disruption of the blood-aqueous barrier (BAB) and promote chronic pathological alterations in AqH, leading to rapid CEnC loss and irreversible corneal edema. We graded the severity of iris atrophy (fig. S1, C to G) as reported previously (*7*) and evaluated the prognosis of corneal transplantation stratifying the patients based on the iris atrophy severity. Consistent with our previous reports (*7*–*12*), in a prospective study excluding patients with immunological graft rejection that can cause bias, the corneal graft survival was poor in patient eyes with severe iris atrophy in two different surgical procedures, endothelial keratoplasty (EK; Fig. 1C and table S1, $P < 0.0001$) and penetrating keratoplasty (PK; fig. S2A, $P = 0.0105$).Next, we found that there was a significant correlation between the severity of iris atrophy and the protein concentration in AqH (Fig. 1D). For all experiments hereafter involving human subjects, ethical approval was provided by all local Institutional Review Board regarding tissue/AqH collection and use, as well as all patients provided informed consent. When these patients underwent corneal transplantation, the preoperative high level of protein in AqH was associated with rapid loss of CEnCs [post-EK, $r = -0.408$, $P < 0.0001$ at 12 months (Fig. 1E); post-PK, $P < 0.03$ at all time points (fig. S2B and table S2)] and shorter graft survival [post-EK, $P < 0.0001$ (Fig. 1F); post-PK, $P = 0.0054$ (fig. S2C)]. Cox proportional hazard models including various clinical factors identified preoperative high AqH protein levels as a significant risk factor for poor graft prognosis (table S3). Because of ethical reasons, we did not obtain postoperative protein levels in AqH. However, even after corneal transplantation, the high protein levels in AqH were expected to be maintained overtime since little recovery was expected once iris atrophy led to BAB disruption due to the poor healing capacity of the intraocular tissues.

Morphological alterations in human CEnC mitochondria

The long-term clinical data suggested that pathological microenvironmental changes in AqH may trigger CEnC dysfunction. Therefore, we sought to elucidate cellular alterations in CEnCs when exposed to the AqH pathological microenvironment and assessed 19 human CEnCs (13 from pathological corneas and 6 from healthy corneas obtained from SightLife Eye Bank, Seattle, WA, USA) using electron microscopy (table S4). A hexagonal CEnC monolayer covering Descemet's membrane was observed in healthy human eyes by scanning electron microscopy (SEM; fig. S2D). In addition, examination of healthy corneal endothelium by transmission electron microscopy (TEM) revealed normal intracellular organelle, including healthy mitochondria with lamellae and cristae structures (Fig. 1, G to H). In contrast, SEM in eyes with bullous keratopathy revealed either a significantly reduced number of CEnCs with irregular dendritic structure (fig. S2E), and almost bared Descemet's membrane with degenerated collagen fibers, or a completely CEnC-bared Descemet basement membrane with degenerated collagen fibers (fig. S2F). Moreover, flattened CEnCs (Fig. 1I) with evidence of damaged mitochondria such as extended vacuolization, electron-dense deposits, and a marked disruption of cristae (Fig. 1J, red arrowheads) were observed by TEM. Compared to healthy CEnCs (fig. S2G), bullous keratopathy CEnCs showed poor staining with MitoTracker Green, as well as mitochondrial vesicle formations (fig. S2H, red arrows). When examined with the mitochondrial membrane potential–dependent dye, JC-1, it was shown that mitochondria in healthy CEnCs maintained membrane potential (Fig. 1K), whereas a number of mitochondria in bullous keratopathy CEnCs lost their membrane potential (Fig. 1L), indicating dysfunctional mitochondria in bullous keratopathy CEnCs. To assess the effect of pathological AqH on CEnC mitochondria in vitro (Fig. 1M), 3 × 3 mm square-shaped pieces of human corneal endothelium were cultured in an AqH cocktail from normal eyes (protein level, 0.466 mg/ml) and in an AqH cocktail from eyes with bullous keratopathy (2.40 mg/ml). JC-1 staining of CEnCs showed normal mitochondrial membrane potential in those cultured in normal AqH cocktail for 48 hours (Fig. 1N) and those cultured in AqH cocktail from bullous keratopathy for 24 hours and then transferred into normal AqH cocktail for 24 hours (Fig. 1O). However, mitochondrial membrane potential became depolarized in CEnCs cultured in AqH cocktails from bullous keratopathy for 24 and 48 hours (Fig. 1, P and Q), showing the direct effect of pathological AqH on mitochondrial membrane potential and also suggesting that the damage can be reversed by culture in normal AqH. It has been shown that CEnCs are vulnerable to mitochondrial stress due to their postmitotic nature and their highly exposed position to ultraviolet light radiation (*13*).

Proteomic analysis of human AqH

The long-term clinical outcome of corneal graft survival showed that the higher the AqH protein levels were, the more likely the corneal graft was to fail, suggesting that alterations at the protein levels may determine the fate of the graft. To identify proteins altered in the pathological AqH, we conducted a proteomic analysis using human AqH (five from bullous keratopathy with iris atrophy and five from healthy eyes) collected during corneal transplantation or cataract surgeries (table S4). After depletion of 14 abundant proteins using the MARS Hu-14 column, followed by tryptic digestion, a quantitative liquid chromatography–mass spectrometry analysis was performed (*14*), and 1162 proteins were identified in AqH. Compared to healthy controls, 265 proteins were found to be significantly changed (elevated, 150 proteins; reduced, 115 proteins) in eyes with bullous keratopathy with non–false discovery rate (non-FDR) and a *P* value less than 0.05 (Fig. 2, A and B). Notably, up-regulation of the complement activation pathway (Fig. 2C) and down-regulation of the glycolytic process (Fig. 2D) were observed in the pathological AqH. Alterations in representative protein levels are given in the obtained heatmap (Fig. 2E). In eyes with bullous keratopathy, Semaphorin 3 and 7 and mitochondrial energy–producing proteins [ATP synthase subunit (ATP5s), nicotinamide adenine dinucleotide phosphate, and propionyl–coenzyme A carboxylase α chain] were significantly decreased, whereas complement factors, such as C1-9, and complement factor H were significantly increased. CD44 levels were also elevated in AqH of bullous keratopathy, which was previously shown to be up-regulated during CEnC culture with inappropriate quality for human CEnC injection therapy (*15*). The protein sets that were significantly elevated in bullous keratopathy AqH samples may regulate important biological pathways such as leukocyte-mediated immunity, immune response, response to stress, defense response, complement activation, and response to stimulus (Fig. 2F). In contrast, the protein sets that were significantly decreased in the same samples are associated with impairment of several metabolic processes such as monosaccharide biosynthetic process, nicotinamide nucleotide metabolic process, cell adhesion, NAD/NADH metabolic process, glycolytic process, and oxidoreduction coenzyme metabolic process (Fig. 2G). The Search Tool for the Retrieval of Interacting Genes/Proteins identified proteolysis (GO0030162, $P = 1.78 \times 10^{-39}$), immune response (GO0006955, $P = 1.05 \times 10^{-24}$), and complement activation (GO0030449, $P = 3.96 \times 10^{-24}$) as biological processes in up-regulated protein networks (Fig. 2H). On the other hand, NAD/NADH metabolic process (GO0019674/0006757, $P = 1.00 \times 10^{-8}$), ATP biosynthetic process (GO0006754, $P = 1.75 \times 10^{-8}$), and glycolytic process (GO0006096, $P = 4.89 \times 10^{-8}$) were identified as biological processes in down-regulated protein networks (Fig. 2I). Hereditary Fuchs' endothelial dystrophy, a major cause of CEnC dysfunction in Western countries and accounting for 4% of the population, has an unaffected AqH and a favorable prognosis for corneal transplantation (*16*). Proteomic analysis in hereditary Fuchs' endothelial corneal dystrophy samples (five eyes) revealed up-regulation of platelet degranulation and canonical glycolysis, which differed from both healthy controls (fig. S3, A to E) and bullous keratopathy samples (fig. S3, F to H).

Transcriptomic analysis of human CEnCs

Mitochondria are more than the energy powerhouse of the cell; they serve as mediators of hypoxic/reactive oxygen species signal transduction, oxidative stress, cellular differentiation, and the cell cycle (*17*). As we have shown above, the TEM images and proteomic approach evidenced mitochondrial damage in CEnCs from bullous keratopathy. We next performed a transcriptomic analysis of CEnCs exposed to pathological AqH. We obtained primary CEnC tissue from 15 patients undergoing corneal transplantation for the treatment of CEnC dysfunction (table S4). As healthy control, CEnC tissue from four corneas obtained from the Seattle Eye Bank were used. Following tissue RNA extraction, we evaluated the quality of RNA for RNA sequencing (RNA-seq). Of 15 eyes with CEnC dysfunction, adequate RNA integrity number (RIN) above 6 was only achieved in seven eyes due to severe CEnC loss in the remaining eight eyes. Therefore, and since we speculated that biological pathway alterations

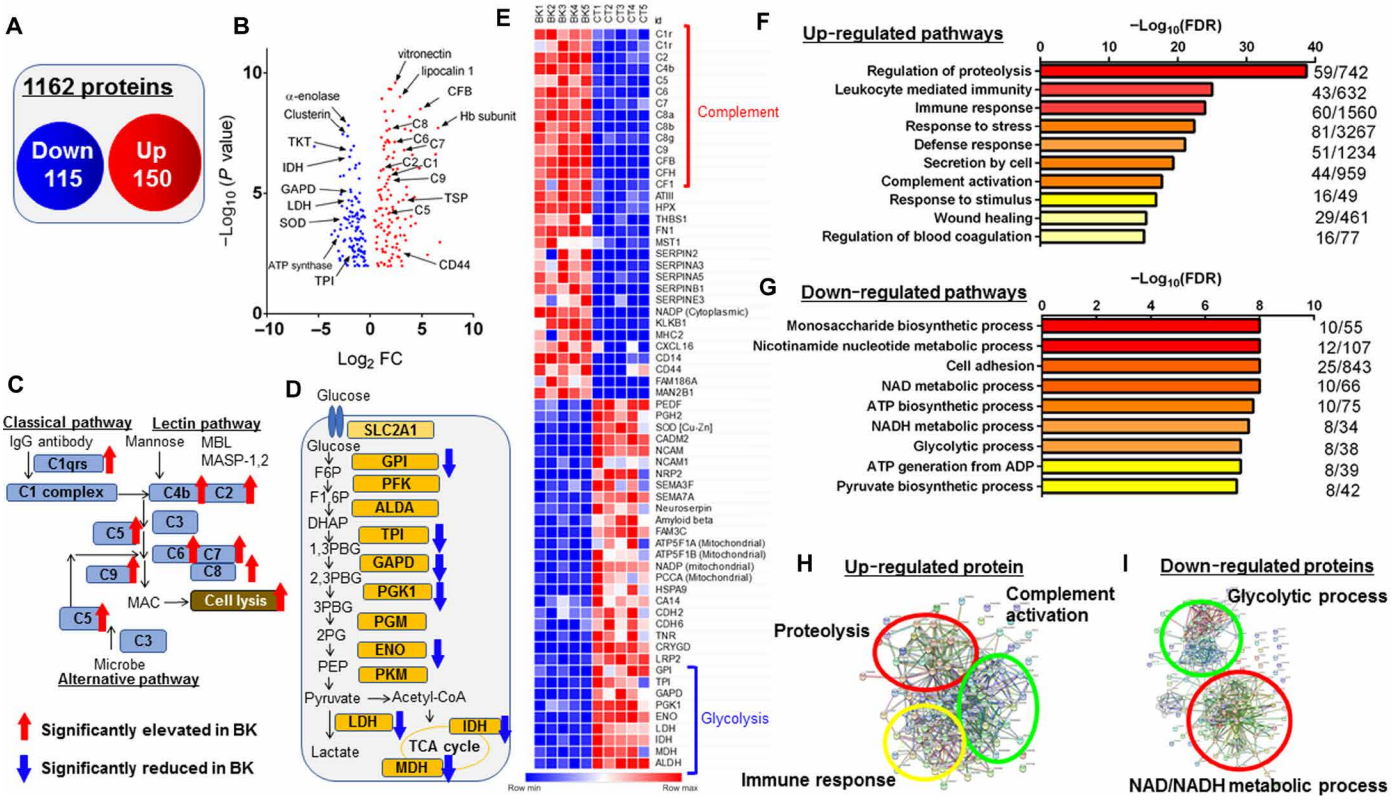

Fig. 2. Proteomic analysis of AqH in bullous keratopathy. (**A**) Venn diagram displaying the number of statistically significant identified altered proteins in eyes with bullous keratopathy. (**B**) The results of FDR ≤ 0.05 (five healthy eyes versus five eyes with bullous keratopathy) depicted on a volcano plot. CFB, complement factor B; GAPD, glyceraldehyde-3-phosphate dehydrogenase; IDH, isocitrate dehydrogenase; LDH, lactate dehydrogenase; SOD, superoxide dismutase; TPI, triosephosphate isomerase; TKT, transketolase; TSP1, thrombospondin1; FC, fold change. (**C** and **D**) Complement factors were significantly elevated in bullous keratopathy as compared to healthy controls (C), whereas the glycolysis-related proteins were significantly decreased (D). IgG, immunoglobulin G; acetyl-coenzyme A, CoA. (**E**) Heat map illustrating quantitative alterations of representative proteins (BK, bullous keratopathy; CT, healthy controls). (**F** and **G**) Canonical biological processes which were significantly up-regulated (F) and down-regulated (G) in bullous keratopathy were characterized using DAVID GO analysis. (**H** and **I**) Functional association network of up-regulated (H) and down-regulated (I) proteins by STRING classification with high confidence (score = 0.700).

must be induced in CEnCs exposed to pathological AqH, we characterized the transcriptional consequences in CEnC of seven individuals undergoing corneal transplantation. We identified 2385 up-regulated and 2880 down-regulated among 40,448 genes (Fig. 3, A and B), which were statistically significant with non-FDR *P* values less than 0.05. Principal components (PC) analysis showed distinct relationships between eyes with CEnC dysfunction and healthy eyes (PC1, 42.0%; PC2, 11.7%; PC3, 9.2%), accounting for 62.9% of the variance observed between gene expression datasets (Fig. 3C). Two of six genes associated with hereditary corneal endothelial dystrophies [zinc finger E-box binding homeobox 1 (*ZEB1*) and solute carrier family 4 member 11 (*SLC4A11*)] were significantly down-regulated in bullous keratopathy CEnCs (down-regulated by 3.0- and 3.7-fold, $P = 6.38 \times 10^{-5}$ and 1.97×10^{-3}, respectively) compared to healthy controls, while four [collagen type VIII α2 chain (*COL8A2*), transcription factor 4 (*TCF4*), lipoxygenase homology domains 1 (*LOXHD1*), and ATP/guanosine triphosphate binding protein like 1 (*AGBL1*)] were not. Whereas CEnCs have minimal expression of cytokine receptors to avoid responding against external stimuli in a steady state (*18*), the gene expression of cytokine receptors, such as interleukin (*IL*)–2r, *IL-4r*, and *IL-17r*, interferon-γr (*IFN-γr*) and apoptosis inducers, programmed cell death ligand (*PD-L2*), and cluster of differentiation 86 (*CD86*), were significantly up-regulated, suggesting that CEnCs may become susceptible to elevated cytokines in AqH of bullous keratopathy (*10*). Furthermore, in line with our electron microscopy findings, mitochondria-related genes, such as creatine kinase mitochondrial (*CKMT*), ATP synthase (*ATPs*), and solute carrier (*SLCs*) genes, were significantly down-regulated in eyes with bullous keratopathy compared to healthy controls (Fig. 3D). Gene transcripts that showed significantly different expression profiles between healthy eyes and eyes with bullous keratopathy were further analyzed for functional Gene Ontology (GO) enrichment, which identified several ongoing cellular components. Genes with significantly higher expression in eyes with bullous keratopathy demonstrated significant enrichment for several functional pathways such as extracellular matrix organization, cell adhesion, integrin-mediated pathway, signal transduction, IFN-γ-mediated pathway, immune response and inflammatory response (Fig. 3E). On the other hand, genes with significantly lower expression in eyes with bullous keratopathy demonstrated significant enrichment for several down-regulated important processes such as canonical glycolysis, glyconeogenesis, PERK-mediated unfolded protein response, glycolytic process, cellular response to hypoxia, response to ischemia, mitochondrial electron transport, and oxidation-reduction process (Fig. 3F).

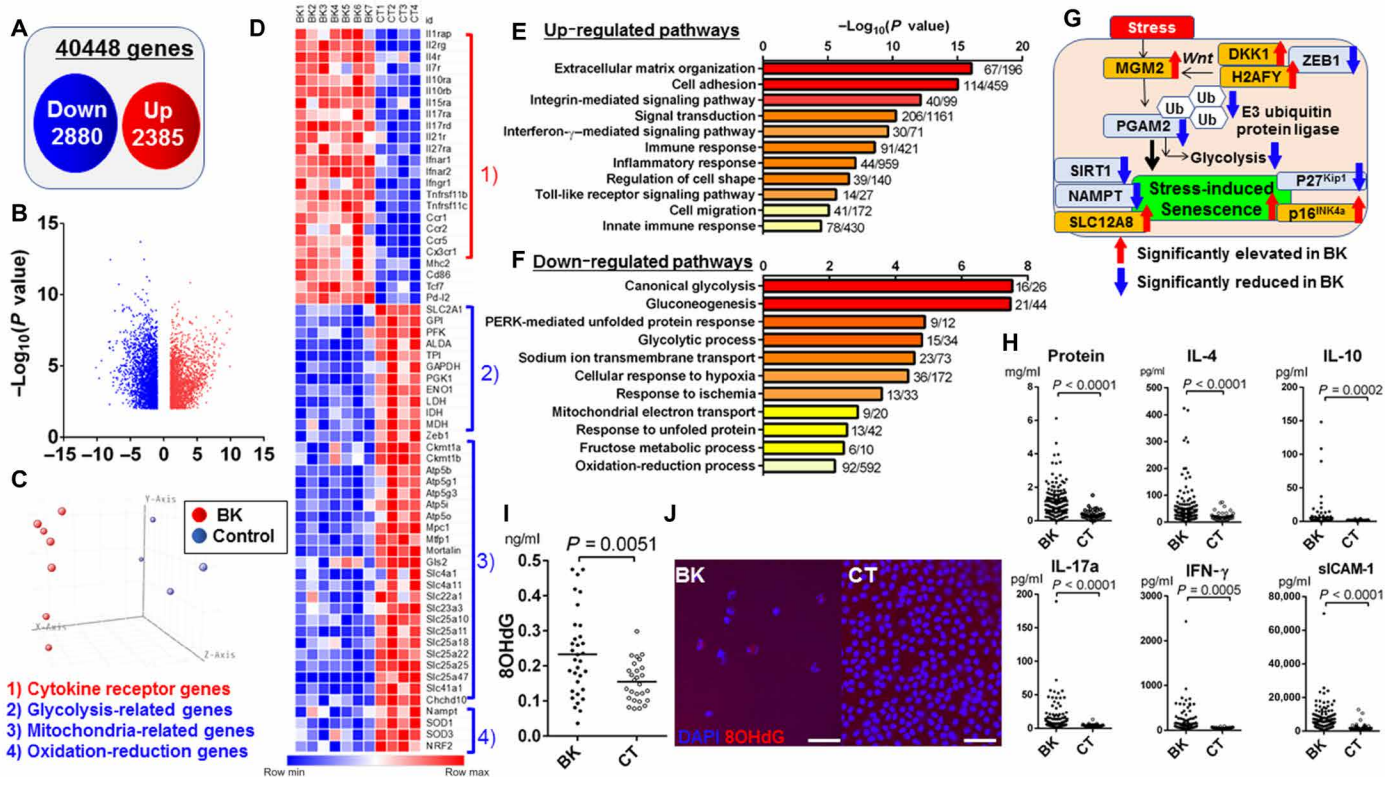

Fig. 3. Transcriptomic analysis of CEnCs in bullous keratopathy. (**A**) Venn diagram displaying the number of statistically significant identified altered genes in CEnCs with bullous keratopathy. (**B**) The principal components analysis results clearly divided healthy and dysfunctional CEnCs (seven eyes with bullous keratopathy versus four healthy eyes). (**C**) The results of FDR < 0.05 (healthy eyes versus bullous keratopathy) depicted on a volcano plot. (**D**) Heatmap illustrating quantitative alterations of representative genes. (**E** and **F**) Canonical biological process were significantly up-regulated (E) and down-regulated (F) in CEnCs of bullous keratopathy were characterized using DAVID GO analysis. (**G**) Significant alterations in the Wnt/MGM2/PGAM2 and SIRT1/NAMPT/SLC12A8 pathways, such as up- and down-regulation of the CEnC senescence markers, $p27^{Kip1}$ and $p16^{INK4a}$, implicated stress-induced senescence in bullous keratopathy. (**H** and **I**) Inflammatory cytokine (H) and 8-OHdG (I) levels were significantly up-regulated in eyes with bullous keratopathy (cytokine, $n = 194$ eyes; 8-OHdG, $n = 33$ eyes) as compared to healthy controls (cytokine, $n = 51$ eyes; 8-OHdG, $n = 27$ eyes; all $P \leq 0.0051$). Unpaired Student's t test. (**J**) Immunohistochemistry of 8-OHdG was positive only in CEnCs of bullous keratopathy. Scale bars, 50 μm. DAPI, 4′,6-diamidino-2-phenylindole.

CEnC cellular senescence markers (*19*) were significantly altered in bullous keratopathy samples ($P16^{INK4a}$, up-regulated by 91.6-fold, $P = 2.43 \times 10^{-6}$; $p27^{Kip1}$, down-regulated by 4.22-fold, $P = 1.07 \times 10^{-7}$), as well as members of the senescence-related MGM2-E3 ubiquitin pathway (Fig. 3G). Furthermore, senescence-related genes, sirtuin 1 (*SIRT1*) and nicotinamide phosphoribosyltransferase (*NAMPT*), which convert NAD^+ to nicotinamide mononucleotide (NMN) (*20*), were also significantly reduced (4.12- and 3.06-fold, $P = 1.28 \times 10^{-6}$ and 7.5×10^{-5}, respectively), whereas solute carrier family 12 member 8 (*SLC12A8*), which was recently identified as a NMN transporter (*21*), was significantly up-regulated in bullous keratopathy CEnCs (2.83-fold, $P = 2.21 \times 10^{-3}$).

To validate the influence of the up-regulation of cytokine receptors, we compared AqH cytokine levels between 194 eyes with bullous keratopathy and 51 healthy eyes using flow cytometric immunobeads assay (table S5) and confirmed significant elevations in cytokine levels for IL-4, IL-10, IL-17a, IFN-γ, and soluble intercellular adhesion molecule 1 (sICAM-1) in bullous keratopathy samples (Fig. 3H). A recent report has demonstrated that elevated levels of IL-10 represent "chronic pathological inflammation" due to negative feedback mechanism (*22*). Similarly, RNA-seq results also indicated higher oxidative stress response in eyes with bullous keratopathy. To test for oxidative stress, we measured the levels of 8-hydroxy-deoxyguanosine (8-OHdG), a critical biomarker for oxidative stress, in AqH using enzyme-linked immunosorbent assay and confirmed significant elevation of 8-OHdG levels in AqH of bullous keratopathy (33 eyes, 0.23 ± 0.12 pg/ml) compared to healthy controls (27 eyes, 0.15 ± 0.06 pg/ml, $P = 0.0051$; Fig. 3I and table S5). Immunohistological evaluation also showed 8-OHdG–positive CEnCs in bullous keratopathy (Fig. 3J).

Development of iris atrophy in DBA2J coincides with CEnCs loss

Through the prospective proteomic and transcriptomic analyses of patient-derived samples, we could accumulate plenty of evidence indicating the tight link among CEnCs, iris, and AqH. To further investigate the cause and effect of these integrative networks, we adopted a murine model to be used by mimicking iris atrophy. The DBA2J mouse strain, which spontaneously develops pigmentary dispersion and iris atrophy (Fig. 4A), is widely used as a murine glaucoma model (*23*). However, little is known on the CEnC state in DBA2J. Immunohistochemical analysis of zonula occludens-1 (ZO-1) in CEnC revealed significant cell loss in DBA2J mice at 20 weeks as compared to those at 6 weeks ($P < 0.0001$), whereas there were no

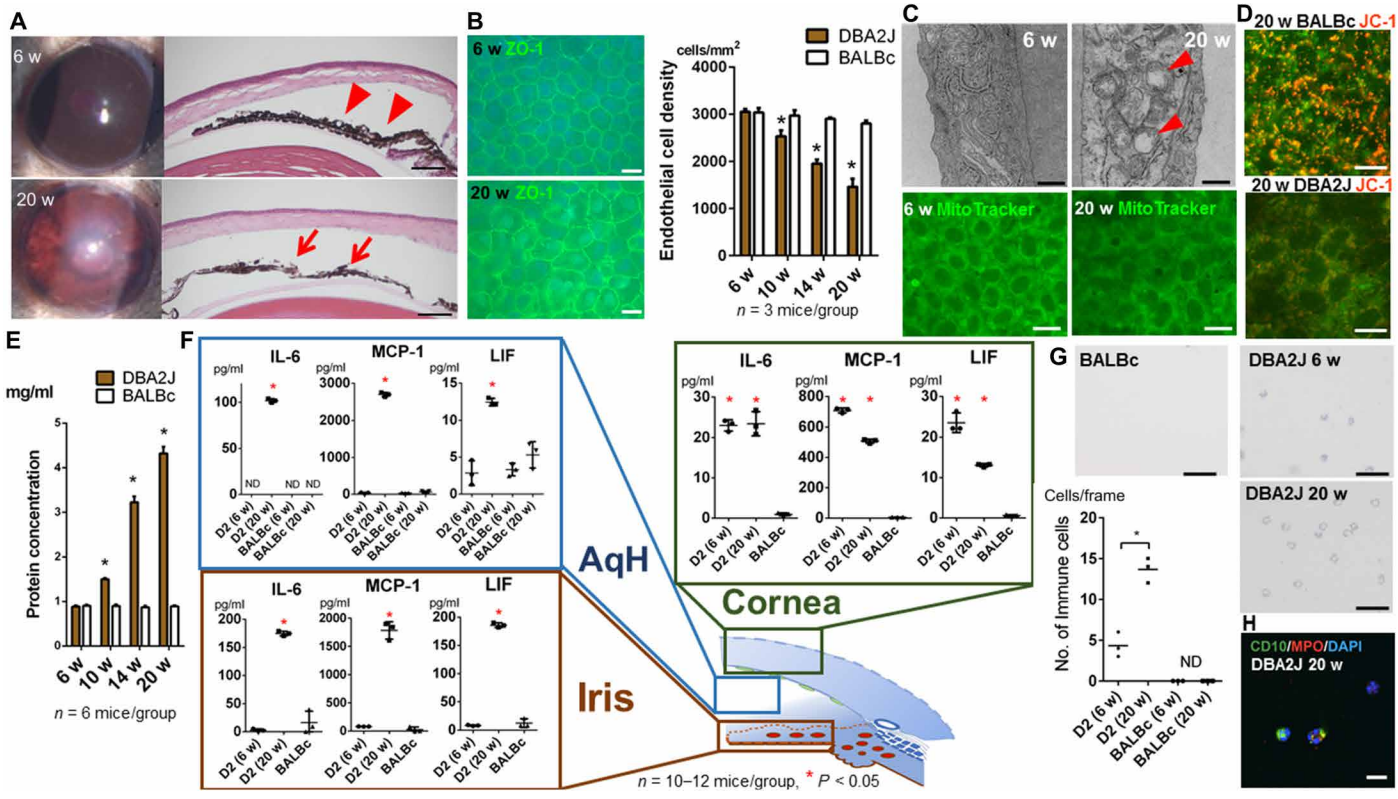

Fig. 4. The DBA2J murine model mimics the human bullous keratopathy pathology. (**A**) Iris structure is normal in DBA2J mice at 6 weeks (red arrowheads); however, iris stromal atrophy spontaneously develops at 20 weeks (red arrows). Scale bars, 100 μm. Photo credit: Kazunari Higa, Tokyo Dental College Ichikawa General Hospital. (**B**) Immunohistochemistry of ZO-1 in DBA2J mice. CECD significantly decreased at 20 weeks in DBA2J mice, whereas no significant difference was noted in BALBc mice (all, $n = 5$ mice). Scale bars, 50 μm. (**C**) Electron microscopy revealed mitochondrial vacuolization at 20 weeks (right, red arrowheads) similar to what was observed in human CEnCs of bullous keratopathy, whereas mitochondria appeared normal at 6 weeks (left). Scale bars, 500 nm. CEnC mitochondrial mass (by MitoTracker) was significantly decreased at 20-week compared to 6-week mice. Scale bars, 20 μm. (**D**) JC-1 staining was decreased in 20-week DBA2J compared to 20-week BALBc mice. Scale bars, 20 μm. (**E**) Protein levels were significantly elevated from 6- to 20-week DBA2J mice (all, $n = 6$ mice, $P < 0.0001$), whereas no statistical difference was observed in BALBc mice. (**F**) AqH IL6, monocyte chemotactic protein-1 (MCP-1), and LIF protein levels were significantly elevated at 20-week compared to 6-week DBA2J mice. Iris IL-6, MCP-1, and LIF protein levels were significantly elevated at 20-week compared to 6-week DBA2J mice (all, $n = 12$ mice, $P < 0.0001$), whereas corneal IL-6, MCP-1, and LIF protein levels were elevated at both 6- and 20-week DBA2J, as compared to BALBc mice. ND, not detected. (**G**) A significant increase in the number of immune cells in the AqH was observed in 20-week compared to 6-week and BALBc mice. Scale bars, 50 μm. Unpaired Student's t test, $^*P < 0.01$. (**H**) Immune cells were positive for CD10 and MPO immunostaining. Scale bar, 10 μm.

significant differences in CECD between 6- and 20-week BALBc control mice (Fig. 4B). Electron microscopy of CEnCs on DBA2J mice at 20 weeks showed mitochondrial vacuolization (Fig. 4C, red arrowheads), which was observed in human samples (Fig. 1J). In addition, MitoTracker staining showed significant loss of mitochondrial mass in 20-week compared to 6-week-old DBA2J mice (Fig. 4C). JC-1 staining revealed loss of mitochondrial membrane potential in 20-week DBA2J compared to 20-week BALBc control mice (Fig. 4D).

We hypothesized that iris atrophy in DBA2J mice could stand as a candidate murine model of CEnC damage induced by iris atrophy and the pathological AqH microenvironment. We measured the protein level in AqH, which showed significant elevation from 0.94 to 4.02 mg/ml at 20 weeks in DBA2J mice ($P < 0.0001$), whereas it stayed around 0.95 mg/ml in BALBc control mice (Fig. 4E). Previous reports showed that the leukemia inhibitory factor (LIF) reduces tight junction and cell survival via signal transducer and activator of transcription 3 (STAT3) signaling in CEnCs (*24*), and high levels of IL-6 and monocyte chemotactic protein-1 (MCP-1) in AqH were associated with rapid CEnC loss after corneal transplantation in human (*10*, *11*). Thus, we assessed protein levels of 14 cytokines in the AqH of DBA2J and BALBc mice using a multiplex bead array assay. The levels of inflammatory cytokines, IL-6, MCP-1, and LIF, in the AqH, were significantly elevated at 20-week DBA2J mice, compared to those of 6-week DBA2J and 6- and 20-week BALBc mice (Fig. 4F). Where did these AqH alterations in protein levels derive from? AqH faces the cornea and the iris. Therefore, we measured protein levels of these cytokines in cornea and iris tissues. IL-6, MCP-1, and LIF protein tissue levels were significantly elevated in the iris at 20-week DBA2J mice, compared to those of 6-week DBA2J and 6- and 20-week BALBc mice (Fig. 4F). Concurrently, these cytokine levels were significantly elevated in the cornea of DBA2J mice both at 6- and 20-weeks, compared to those in BALBc mice, demonstrating a similar elevation pattern of cytokines in the iris and the AqH. These increases of inflammatory cytokines can recruit immune cells into the AqH. Therefore, we collected AqH cellular aggregates after centrifuging of AqH from 20-week-old DBA2J mice, which contained significant number of immune cells (Fig. 4G), compared to 6-week-old DBA2J mice ($P < 0.0001$). In contrast, there were no immune cells in AqH from those of BALBc mice. We also tested the cellular components in human AqH. The cell pellet smear from bullous

keratopathy samples showed significantly increased number of immune cells in AqH, whereas no cells were detected in AqH of healthy controls (fig. S4, A to C; $P = 0.0005$). The immune cells in the AqH were positive for CD10 and myeloperoxidase (MPO) both in DBA2J (Fig. 4G) and human patients (fig. S4D), indicating that they are neutrophils. The clinical relevance of cytokines in AqH has been already emphasized regarding the prognosis of corneal transplantation (*9*–*12*). However, to date, the source of cytokines in AqH remains elusive. These results collectively suggest that the atrophic iris tissue contains similar cytokine components, inducing immune cell recruitment into AqH. Since DBA2J is a murine model for pigmentary dispersion glaucoma, to exclude the possibility that glaucoma development might affect our results, we therefore measured intraocular pressure (IOP), which was shown to remain at normal levels until 20 weeks (fig. S5A). All these phenotypes observed in DBA2J mice resembled those of bullous keratopathy in humans, suggesting that elevated inflammatory protein levels in AqH coincided with iris atrophy and immune cell recruitment, which might cause CEnC damage in DBA2J mice.

Transplantation of DBA2J CEnC layer into BALBc anterior chamber

Despite all indications to the contrary, CEnC loss could be attributable to an unidentified DBA2J phenotype independent of AqH and not associated with microenvironmental alterations in AqH. To demonstrate the direct association between CEnC damage and the pathological AqH microenvironment in DBA2J mice, we next transplanted the cornea of 20-week DBA2J mice into the anterior chamber of young BALBc/DBA2J mice and vice versa (Fig. 5A). After removing the corneal epithelium, wedge-shaped corneal grafts (approximately 0.3 mm × 1.5 mm) were transplanted into the anterior chamber of the recipients and lifted with air injection beneath the grafts (*25*). All syngeneic (from young to old and from old to young DBA2J mice) and allogeneic transplants from BALBc to DBA2J mice failed within 1 to 7 days. In contrast, allogeneic transplants from DBA2J to BALBc mice successfully survived (Fig. 5B, $P < 0.0001$). We confirmed that the graft failure was caused by the decreased density of CEnCs in the graft (Fig. 5, C and D). CECD of the 20-week DBA2J corneal grafts was significantly decreased after transplantation

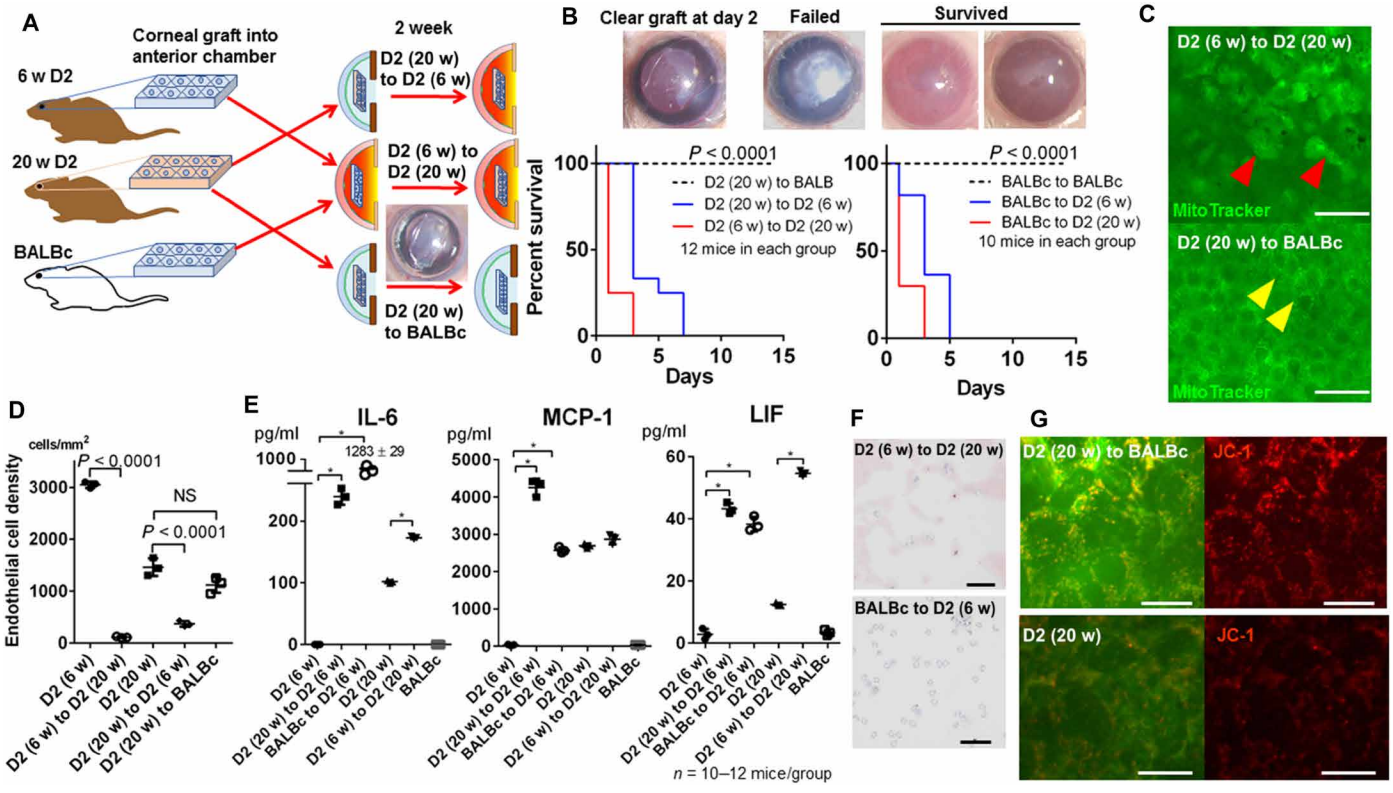

Fig. 5. Convalescence of DBA2J CEnCs when transplanted into BALBc mice. (**A**) Corneal endothelial tissues were transplanted from 6- and 20-week DBA2J into 6-, 20-week DBA2J, or BALBc mice to evaluate whether CEnC damage in DBA2J mice is due to the pathological AqH microenvironment secondary to the atrophic iris. Unexpectedly, 6-week DBA2J mice developed severe inflammation after syn-/allogeneic grafts, and all ended in graft failure. (**B**) Representative images of corneal grafts. Failed grafts became white and edematous. DBA2J (syngeneic) and BALBc (allogeneic) grafts into DBA2J mice failed within a week despite the absence of apparent immunological rejection, whereas grafts into BALBc mice successfully survived ($n = 10$ to 12 mice, log-rank Mantel-Cox test, $P < 0.0001$). Photo credit: Kazunari Higa, Tokyo Dental College Ichikawa General Hospital. (**C** and **D**) To confirm whether graft failure was due to corneal endothelial decompensation, we assessed graft CEnCs by mitochondrial staining (MitoTracker). Failed grafts exhibiting mitochondrial vacuolization (red arrowheads) and decreased number of CEnCs. Notably, CEnCs transplanted from 20-week DBA2J to BALBc mice were normal (yellow arrowheads). Scale bars, 50 μm. NS, not significant. (**E**) Cytokine levels in AqH after corneal transplantation were measured using a multiplex immunobead assay. Cytokine levels were significantly elevated in eyes with failed grafts (DBA2J/BALBc to DBA2J), whereas in eyes with survived grafts (DBA2J to BALBc). Unpaired Student's *t* test, $^*P < 0.01$. (**F**) Immune cells numbers in AqH after corneal transplantation remained at the same levels in 20-week DBA2J mice compared to those in a steady state, whereas they were significantly increased in eyes with allogeneic transplantation (BALBc to DBA2J), in which cytokine levels were extraordinarily elevated. Scale bars, 50 μm. (**G**) JC-1 staining revealed that mitochondrial membrane potential was reversed in grafts transplanted from 20-week DBA2J to BALBc compared to naïve 20-week DBA2J mice. Scale bars, 20 μm.

into the anterior chamber of 6-week DBA2J mice and vice versa ($P < 0.0001$), whereas it remained stable when transplanted into the anterior chamber of BALBc mice. We expected that the corneal grafts would survive into young DBA2J mice as these had normal protein levels in the steady state (Fig. 4E). However, they all clinically developed iris pigment dispersion and failed. Therefore, to determine the alterations in AqH microenvironment, we measured cytokine levels after corneal transplantation. We found that the IL-6, MCP-1, and LIF levels in AqH significantly increased after corneal transplantation in 6-week DBA2J mice (Fig. 5E, $P < 0.0001$), indicating that the DBA2J is hypersensitive to minimally invasive operation and alters AqH environment inflammatory (*26*). In 20-week DBA2J mice after syngeneic transplantation, IL-6 and LIF levels were moderately elevated compared to those in a steady state; however, the number of immune cells did not increase (Fig. 5F), suggesting that CEnCs decreased due to humoral factors in AqH rather than cellular reactions. In the allogeneic transplantation from BALBc to DBA2J mice, IL-6 level in AqH was significantly increased up to 1283 ± 29 pg/ml as well as the number of immune cells in AqH (Fig. 5F). CEnCs of the graft transplanted from 20-week DBA2J to BALBc mice showed increased mitochondrial potential, compared to that of 20-week DBA2J (Fig. 5G), which suggests that pathological CEnC mitochondrial alterations in old DBA2J mice can be reversed, and CEnCs can turn to normal when transplanted into a healthy microenvironment.

DISCUSSION

The current study identified several biological processes that were up- and down-regulated in the human AqH and CEnCs. Further, electron microscopy revealed that CEnCs in bullous keratopathy exhibited serious mitochondrial stress with severe loss of cristae and abnormal vacuolization. Recently, we showed that preoperative cytokine levels in AqH were correlated with CECD after corneal transplantation (*8*–*11*), suggesting that the pathological microenvironment in AqH induces CEnC apoptosis. However, the exact mechanism remains elusive. The multiomics approaches from human samples suggested the following mechanisms: First, iris atrophy results in BAB disruption and elevated protein levels, with concurrent complement activation and oxidative stress in the AqH. Second, because of chronic exposure to such altered AqH environment, the cytokine receptors are up-regulated in CEnCs despite their minimal expression in steady state. Simultaneously, the abnormal AqH induces down-regulation of glycolysis, intracellular respiration, and NAD/NADH metabolism in the CEnCs, leading to mitochondrial degeneration, and lastly, to CEnC loss (Fig. 6).

Previous histopathological studies have reported degeneration, decrease, or absence of CEnCs in patients with bullous keratopathy (*27*). However, little was known about organelle changes and their relation to cellular biological processes under pathologic conditions. Consequently, our current observations raise the question: Is the exhibited mitochondrial ultrastructure in our study (loss of cristae and vacuolization) specific to bullous keratopathy cases? On the basis of literature review of various types of diseases, it is made apparent that mitochondrial ultrastructure varies widely among pathologies. Regarding mitochondrial diseases, in Leber's hereditary optic neuropathy, the mitochondria occupying the cytoplasm were filled with stacked cristae ("mitochondria stream"), whereas, in chronic progressive external ophthalmoplegia, mitochondria were swollen and had lost inner cristae exhibiting an "onion-ring appearance" (*28*). On the other hand, TEM revealed abnormal endoplasmic reticulum and severely swollen mitochondria in Fuchs' endothelial corneal dystrophy (*29*).

Recent studies have revealed that mitochondria are not only the energy powerhouse of the cell but also serve as mediators of cell signaling, regulation of metabolism, cell cycle control, development, antiviral responses, and cell death (*17*). In line with the abnormal mitochondrial ultrastructure, CEnC transcriptomic results showed

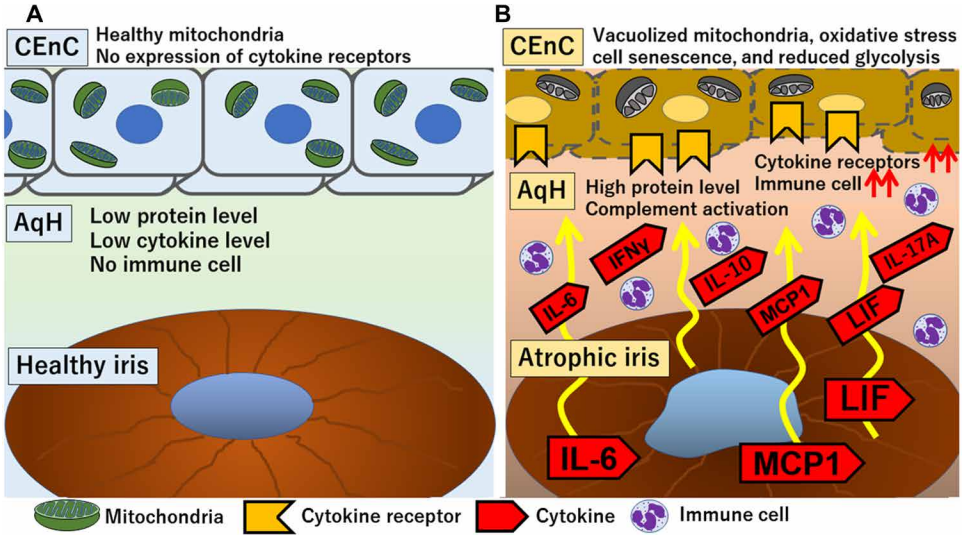

Fig. 6. Comprehensive mechanism of bullous keratopathy development. (**A**) Healthy iris pigmentary epithelial cells in a steady state exhibit immunomodulatory property. Protein and cytokines levels in AqH are normal, and no immune cells are present. Thus, CEnCs are kept healthy. (**B**) In bullous keratopathy eyes with atrophic iris, iris tissue produces high levels of cytokines, such as IL-6, MCP-1, and LIF, which are released into AqH, and, in turn, recruit immune cells into AqH. Atrophic iris also results in the breakdown of the BAB. Subsequently, proteins, cytokines, and complement factor levels in AqH increase. Chronic exposure to this AqH environment leads to up-regulation of cytokine receptors expression in the surface of CEnCs. Such pathological microenvironment alterations lead to mitochondrial vacuolization, increased oxidative stress, cellular senescence, and reduced glycolysis inside CEnCs, which lastly ends in loss of CEnCs.

alterations in various genes reported to lead to mitochondrial dysfunction. Both *ZEB1 and SLC4A11*, genes that are responsible for hereditary corneal endothelial dystrophies, were significantly reduced in CEnCs of bullous keratopathy compared to controls. *ATP5* genes, which are subunits of ATP synthetase and regulate SIRT3 to restore mitochondrial function in response to stress, were also significantly reduced (*30*). *CKMT1* is another important gene for global cell metabolism, including purine metabolism, amino acid metabolism, and energy metabolism (tricarboxylic acid cycle and glycolysis), and its suppression renders mitochondria dependent on creatine pathway activity for ATP production (*31*). The coiled-coil-helix coiled-coil helix domain containing 10 (*CHCHD10*), which is an amyotrophic lateral sclerosis causative gene and can single handedly promote loss of cristae junction with impaired mitochondrial genome maintenance after oxidative stress (*32*), was significantly down-regulated (3.70-fold, $P = 3.53 \times 10^{-5}$). Further, the solute carrier family 25 member 25 (*SLC25A25*), gene absence of which leads to energy insufficiency in the cell and leads to reduced physical endurance (*33*), was significantly down-regulated in CEnCs of bullous keratopathy (6.19-fold, $P = 1.64 \times 10^{-7}$). *SLC25A25* is a Ca^{2+}-sensitive ATP-Mg^{2+}/P_i carrier in the inner mitochondria membrane, which plays an important role in the regulation of ATP homeostasis necessary to support Ca^{2+} cycling (*33*). Research on the biology of NAD^+ cofactor has provided many critical insights into the pathogenesis of age-associated diseases (*20*). Supplementing NAD^+ intermediates, such as NMN, yields preventive and therapeutic effects, ameliorating age-associated pathophysiologies and diseases, such as diabetes mellitus, retinal/neuronal ischemia, dementia, and heart diseases by improving mitochondrial function (*20*).

It has been reported that allogeneic skin grafts from DBA2 to BALBc were all rejected within 14 days (*34*). The results of graft survival from DBA2 to BALBc in the current study suggested an ocular specific mechanism, such as anterior chamber–associated immune deviation (ACAID) (*25*). The endothelial lamellar keratoplasty procedure used in the current study is reported to induce ACAID (*26*). Moreover, this minimally invasive procedure without any corneal sutures causes almost no surgery-induced inflammation (Fig. 5B). In contrast, conventional full thickness keratoplasty is relatively invasive, needing removal of corneal sutures at 7 days to prevent inflammation and neovascularization. Furthermore, after full thickness keratoplasty from DBA2J to BALBc, the graft survival rate is reported to be 0% due to immunological rejection (*35*), which can cause significant reduction in CECD (*36*). Thus, we selected endothelial lamellar keratoplasty in the current study.

Regarding its ocular phenotype of DBA2J, Chang *et al.* (*23*) first reported severe iris atrophy and pigment dispersion glaucoma. They also mentioned that iris abnormality in DBA2J resembles ICE syndrome, essential iris atrophy, and A-R syndrome in human, which develop corneal endothelial decompensation and have an extremely poor graft prognosis after cornel transplantation. The DBA2J phenotype is reported to be caused by mutations in the glycoprotein Nmb (*Gpnmb*) and tyrosinase-related protein 1 (*Tyrp1*) genes. *Tyrp1* encodes a component of a melanosomal membrane protein complex involved in pigment production, whereas *Gpnmb* is less characterized but also presents in melanosomes (*23*). The corneal transplant results in this study (DBA2J to BALBc) demonstrated a reversible CEnC change, suggesting direct damage of CEnCs by the pathological AqH environment in DBA2J mice. Thus, we propose that CEnC damage is associated with the pathological iris alterations and subsequent microenvironmental changes in the AqH and suggest that CEnC damage can be reversed by adjusting the AqH microenvironment appropriately.

Innate immunity plays a major role in resistant to tolerance induction and further amplifies graft-specific adaptive immunity, although innate immune mechanisms are not sufficient to lead to graft rejection (*37*). In solid organ transplantation, ischemia/reperfusion injuries initiate innate immunity, which, in turn, enhances immunogenicity through the activation of antigen-presenting cells (*37*). In contrast, in the cornea, deprivation of immune privilege has been well-investigated through the activation of adaptive immunity, such as induction of neovascularization. However, innate immunity in the cornea is still elusive. In the current study, severe inflammation leading to syngeneic graft dysfunction in DBA2J mice is not antigen-specific adaptive immunity but can be a neutrophil-mediated innate immune response. This response was exacerbated in allogeneic BALBc grafts into DBA2J AqH. Preactivated innate immunity in the AqH with iris atrophy (elevated protein levels, the presence of neutrophil, complement activation, etc.) suggested from human experiments is still needed for further studies, especially in relation to immune privilege and humoral factors leading to loss of CEnCs and corneal graft failure. Together with clinical studies, we believe that DBA2J can serve as a suitable model for the future studies to specify therapeutic molecules.

This study had some limitations, the lack of a therapeutic angle, for instance. However, the use of DBA2J murine model in ocular studies provides several benefits. At first, a murine model will help us clarify the spatiotemporal biological processes, since differentiating primary pathological causes and secondary responses has been difficult in humans due to ethical reasons. Second, immune responses and wound healing capacity are kept to a minimum without being influenced by systemic conditions, given its immune privileged status; thus, this model can be a good candidate to investigate the relationship between microenvironmental alterations and cellular response in vivo. Third, we have direct access to the cornea with minimal surgical manipulation, which will enable us to conduct clinical evaluations and intravital imaging for cellular responses to develop therapeutic interventions in the future.

We propose a mechanism whereby the inflamed state of AqH leads to up-regulation of cytokine receptors and Wnt signaling in CEnCs, resulting in the stress-induced senescence of CEnCs (Fig. 3G). CEnCs have unique properties. For example, human CEnC longevity exceeds 100 years without cell division. In addition, human CEnC numbers decrease gradually; their loss takes years in chronic senescence process. There is increasing evidence suggesting that cellular senescence is accelerated through complement-mediated Wnt signaling (*38*) and down-regulation of Sirtuins/NAD^+ metabolic pathway (*21*, *22*, *31*). Bullous keratopathy and graft failure due to CEnC loss are sight-threatening complications arising in some of the most common forms of blindness treatment procedures, such as cataract, glaucoma, and retinal surgeries. These results we have shown here warrant clinicians to avoid iris damage during surgeries, to prevent development of bullous keratopathy with poor prognosis for corneal transplantation. The current study also showed that the pathological microenvironment alteration resulting from iris atrophy following these intraocular surgeries can accelerate the stress-induced senescence of CEnCs and CEnC loss. Future spatiotemporal studies will further elucidate the association between stress-induced senescence and cell survival of CEnCs. In addition, understanding the mechanism

behind these pathologies may allow clinicians/eye banks to optimize the corneal donor tissues for patients undergoing corneal transplantation. That is, donor CEnCs from 90-year-old individuals can survive for several decades in young recipients' eyes under healthy conditions (such as keratoconus), whereas, in challenging eyes with severe iris atrophy, such as in A-R syndrome and ICE syndrome, CEnCs from 20-year-old donors may survive longer than those from 90-year-old donors. Corneal tissue is one of the limited medical resources, especially in Asian countries, as the number of donors is still small compared to that of waiting patients. Selecting corneas from younger donors to be transplanted to individuals with complicated bullous keratopathy and severe iris atrophy may prolong graft survival rates. Moreover, the average age of donors is increasing in Japan, which is a potentially serious problem for long-term prognosis of corneal transplantations. Social action to inform the public and share this knowledge will contribute to increased donor numbers from the younger generation, which we believe will improve overall prognosis in worldwide corneal transplantations.

MATERIALS AND METHODS

Study design

The end goal of this study was to identify the role of the iris atrophy–induced pathological AqH microenvironment in CEnC dysfunction and loss and further demonstrate DBA2J as a murine model of CEnC loss, which will help evaluate the underlying spatiotemporal pathological mechanism in the future. The clinical procedures, outcomes, and associated laboratory methods for cytokine measurement have been reported in detail previously (*8*–*12*). By analyzing protein and cytokine levels in the AqH from patients with bullous keratopathy versus a control cohort (uncomplicated cataract), we evaluated their influence on the long-term prognosis of corneal transplantation. Stored AqH samples and clinical data were analyzed after 3-year clinical observations were completed. We subsequently used the DBA2J mouse strain, which spontaneously develops iris atrophy as a model of CEnC loss. In patients with bullous keratopathy undergoing corneal transplantation, CEnC loss, a critical factor for long-term prognosis, can be influenced by donor factors (age, sex, the presence of diabetes, history of intraocular surgeries, etc.), surgical factors (surgeons' experience, surgical time, simultaneous procedures, etc.), and recipient factors (age, bullous keratopathy etiologies, iris atrophy, diabetes, and history of glaucoma). Thus, we evaluated the various parameters (CECD and protein/cytokine levels), estimated SE and *P* values from the Student's *t* test and Spearman's correlation coefficients, based on previous reports, and determined sample size.

Clinical study

A prospective clinical study on long-term prognosis of corneal transplantation related to iris atrophy and AqH was conducted in Tokyo Dental College Ichikawa General Hospital from October 2015 to June 2019 in accordance with the Declaration of Helsinki. The study was approved by the Institutional Ethics Review Board of Tokyo Dental College (I15-42R, I15-44, and I17-78). Written informed consent was obtained from all participants before the interventions. Iris atrophy severity was defined as iris depigmentation, laser iridotomy, or iris defect due to intraocular surgeries (*7*). The severity grade of iris atrophy for each case was determined on the basis of its severity from slit- lamp findings in a blinded manner by one of two corneal specialists (T.Y. or Y.Y.-Y.). Briefly, normal eyes are regarded as "no iris atrophy" (fig. S1C), eyes with "mild iris atrophy" are defined as iris atrophy limited to only one (fig. S1D) to two quadrants (fig. S1E), and eyes with "severe iris atrophy" are defined as iris atrophy from three (fig. S1F) to four quadrants (fig. S1G).

Patient demographics

The etiologies of patients undergoing EK included pseudophakic/aphakic bullous keratopathy (PBK/ABK, 152 eyes), Fuchs' endothelial corneal dystrophy (20 eyes), and those undergoing PK included PBK/ABK (63 eyes), corneal scar (27 eyes), keratoconus (10 eyes), and hereditary corneal dystrophies (2 eyes). Comorbidity of glaucoma was significantly high in eyes with iris atrophy. In patients undergoing EK, glaucoma was present in seven patients without iris atrophy (13.0%), in 17 patients with mild iris atrophy (IDA1-2, 25.4%), and in 21 patients with severe iris atrophy (IDA3-4, 52.3%; χ^2 test, $P < 0.0001$). In patients undergoing PK, glaucoma was present in 4 patients without iris atrophy (9.5%), in 8 patients with mild iris atrophy (30.8%), and in 12 patients with severe iris atrophy (35.3%; $P = 0.188$). The number of previous intraocular surgery was 1.6 ± 1.4 (0 to 9) in eyes undergoing EK and 1.9 ± 1.6 (from 0 to 9) in eyes undergoing PK. The protein levels in AqH was significantly correlated with the number of previous intraocular surgery [$r = 0.419$ (in EK) and 0.575, both $P < 0.0001$]. Topical steroids were prescribed in 47 patients (27.3%) before EK and 30 patients before PK (29.4%).

Corneal transplantation procedures and postoperative management

We performed corneal transplantation, conventional PK, and modern lamellar keratoplasty, Descemet stripping automated endothelial keratoplasty (DSAEK), in a standard fashion as previously described (*9*–*12*). Both after PK and DSAEK, all patients were prescribed the eye drops levofloxacin (Santen, Osaka, Japan) and betamethasone 0.1% eye drops (Santen) for use five times a day. Topical betamethasone eye drops were tapered over the following 6 months. At 6 months post-PK and DSAEK, we prescribed 0.1% fluorometholone eye drops (Santen) three times a day for up to 12 months after surgery, then tapered to two times a day, and continued to prevent graft rejection overtime. Some patients had mild IOP elevation more than 21 mmHg (43 patients after EK and 41 patients after PK), which resolved with topical antiglaucoma agents and management with topical steroids. Three patients underwent glaucoma surgery due to refractory IOP elevation after PK and were excluded from the study. Twelve patients who developed graft rejection (nine patients after PK and three patients after DSAEK) during follow-up and were also excluded from the study. We excluded from the correlation analyses eight eyes in which air injection was performed for the treatment of postoperative double chamber, due to air injection being associated with CECD loss after corneal transplantation.

Electron microscopy

Samples for electron microscopy observation were prepared as previously described (*39*). Briefly, human corneas were primary fixed with 2.5% glutaraldehyde for 12 hours at 4°C. Pinned corneas on silicone sheet were washed with 0.1 M phosphate buffer (pH 7.4) (Muto Pure Chemicals, Tokyo, Japan) and postfixed with 1% osmium tetroxide (OsO_4, TAAB Laboratories Equipment Ltd., England, UK) at 4°C, dehydrated in a series of increasing concentrations of ethanol and in 100% ethanol in the final dehydration step. Human corneal samples were dissected into several pieces for TEM and also for SEM. For TEM observation, dehydrated cornea samples were

soaked in acetone (Sigma-Aldrich, MO, USA), with *n*-butyl glycidyl ether (QY1, Okenshoji Co. Ltd., Tokyo, Japan), then in graded concentration of Epon with QY-1, and embedded into 100% Epon [100 g of Epon is composed of 27.0 g *N*-methyl-4-nitroaniine, 51.3 g of EPOK-812, 21.9 g of dodecenyl succinic anhydride, and 1.1 ml of 2,4,6-tris(dimethylaminomethyl)phenol all from Okenshoji Co. Ltd., Tokyo, Japan] for 12 hours. Infiltration of pure Epon was enhanced for 48 hours at 4°C. Polymerization with pure Epon was completed for 72 hours at 60°C. The ultrathin sections with 70-nm thickness were prepared on the copper grids with an ultramicrotome (Leica UC7, Leica Biosystems, Wetzlar, Germany) and stained with uranyl acetate and lead citrate for 10 min each. Sections were observed under an electron microscope using TEM (JEM-1400plus, JEOL, Tokyo, Japan). For SEM analysis, cornea samples were freeze-dried with 100% t-butyric alcohol (VFD-21S, Vacuum device, Ibaraki, Japan). The specimens attached to the aluminum stage with double-sided carbon tape and carbon paste were coated with platinum and palladium using conductive heavy metal coater at a current of 6 mA for 90 s (SC-701, Sanyu Electron Co. Ltd., Tokyo, Japan) and observed using SEM (SU6600, Hitachi High-Tech, Tokyo, Japan).

CEnCs culture in normal and pathological AqH cocktails

For in vitro experiment, AqH cocktails were prepared from AqH collected at the beginning of 15 normal cataract surgeries (normal AqH cocktail; protein level, 0.466 mg/ml) and AqH collected at the beginning of 23 corneal transplantations for the treatment of bullous keratopathy (bullous keratopathy AqH cocktail; protein level, 2.40 mg/ml). Human corneal endothelial tissues imported from CorneaGen (Seattle, WA, USA) were carefully cut into 3 mm × 3 mm pieces using disposable blades. Corneal endothelial tissues were cultured in 150 μl of normal and bullous keratopathy-AqH cocktails at 37°C for 48 hours and stained using JC-1 (#924, MitoPT JC-1, ImmunoChemistry Technologies, Bloomington, MN, USA). To assess whether mitochondrial membrane potential is reversible, AqH cocktails were exchanged from normal to bullous keratopathy and vice versa at 24 hours during culture and stained using JC-1 at 48 hours.

Proteomic analysis

A total of 15 AqH samples were collected during corneal transplantations or cataract surgeries (five eyes with bullous keratopathy, five eyes with Fuchs endothelial corneal dystrophy, and five cataract eyes without comorbidity; table S4). The AqH samples were centrifuged at 3000*g* for 3 min, and the soluble fractions were collected and stored at −80°C until measurement. After depleting abundant proteins using MARS Hu-14 column (Agilent, Santa Clara, CA, USA), proteins were reduced, alkylated, and lastly digested with 5 μl of immobilized trypsin (Thermo Fisher Scientific, Waltham, MA, USA) with shaking at 1000 rpm at 37°C for 6 hours. After removal of sodium deoxycholate and sodium *N*-lauroylsarcosinate, the resulting peptides were desalted and subjected to mass spectrometric analysis. Peptides were analyzed by Orbitrap Fusion Lumos mass spectrometer (Thermo Fisher Scientific). Protein identification and label-free quantification analysis were performed with Proteome Discoverer 2.2 software (Thermo Fisher Scientific). The tandem mass spectrometry spectra were searched against the *Homo sapiens* protein database in SwissProt (www.nextprot.org/), with an FDR set to 1% as an identification filter. For the AqH protein analysis, all detected peaks were standardized by adjusting the median value to 1.0×10^4. GO analysis was conducted using DAVID (https://david.ncifcrf.gov/tools.jsp) and STRING (https://string-db.org/).

Transcriptomic analysis

Corneal endothelium was stripped and collected either from patient eyes with bullous keratopathy during EK or from Eye Bank eyes (SightLife, Seattle, WA, USA). In both procedures, the endothelium is routinely discarded. The removed endothelium was immediately submerged in TRIzol (15596-026, ThermoFisher Scientific) in ribonuclease (RNase)–free 1.7-ml Eppendorf tubes and subsequently used for RNA-seq. The miRNeasy Micro Kit (Qiagen, Valencia, CA, USA) was used to extract tissue RNA, following the manufacturer's instruction. RNA quality was checked using a NanoDrop (Thermo Fisher Scientific) and Bioanalyzer RNA 6000 pico chip (Agilent). Samples with RIN values above 6 were chosen for further analysis. Twelve samples were used for RNA-seq including seven bullous keratopathy and four healthy controls (table S5). RNA samples were prepared using the NEBNext Ultra II Directional RNA Library Prep Kit for Illumina (New England Biolabs Inc., Ipswich, MA, USA). The libraries were sequenced on a NextSeq (Illumina, San Diego, CA, USA) using a 75–base pair (bp) paired-end read high output v2 run. This produced 20 to 25 M paired-end reads per sample. We mapped the 75 nucleotide reads to human genome (University of California Santa Cruz Human hg19; https://genome.ucsc.edu/) using TopHat2 (ver 2.1.1; https://ccb.jhu.edu/software/tophat/index.shtml) and the Bowtie aligner (ver 2.3.2.0; http://bowtie-bio.sourceforge.net/bowtie2/manual.shtml), allowing up to 2-bp mismatches per read (default position). StrandNGS (ver 3.2; www.strand-ngs.com/) was used to generate counts of reads uniquely mapped to known and annotated genes using RefSeqGene (2015.10.05; www.ncbi.nlm.nih.gov/refseq/rsg/). A normalization factor was calculated using the trimmed mean of M values method, and the dispersion parameter for each gene was estimated with the Cox-Reid common dispersion method. Testing for differential expression used a negative binomial generalized linear model for each gene. The Benjamini-Hochberg correction was used to correct for multiple comparison with an FDR of 0.05. GO analysis was conducted using DAVID.

Animal experiment and transplantation surgery

This study adhered to the Association for Research in Vision and Ophthalmology statement for the Use of Animals in Ophthalmic and Vision Research. Six- to 20-week-old mice were purchased from Charles River Laboratories (Yokohama, Japan). We used 6- to 24-week-old BALBc mice (H-2d, Igh-Ca, CD52, and CD8a2), C57BL/6 mice (H-2b, Qa-1b, and Ly-92), and DBA2 (H-2d, Igh-Cc, CD51, and CD8a1). The donors and recipients represented minor antigen disparities in BALBc/DBA2J transplantation and minor antigen/major histocompatibility complex disparities in C57BL6/DBA2J transplantation. Each animal was deeply anesthetized with an intraperitoneal injection of medetomidine (0.15 mg/kg), midazolam (2 mg/kg), and butorphanol (2.5 mg/kg) before surgical procedures. Endothelial lamellar keratoplasty were performed as reported previously (*25*). Briefly, after complete removal of corneal epithelium by scraping, central corneas from normal eyes of DBA2J and BALBc donors were excised and cut using Vannas Scissors (Inami Inc., Tokyo, Japan) into wedge-shaped fragments measuring approximately 0.4 mm × 1.5 mm. Individual fragments were then inserted into the anterior chamber through an oblique incision and placed onto the center of the recipient endothelium by injecting a small air bubble. The mice with decentered or iris-touched grafts were excluded. Fourteen days after the procedure, corneas were excised for immunohistochemical (ZO-1), MitoTracker (M7514, Thermo Fisher Scientific),

and JC-1 imaging analyses. Intraocular pressure in mice was measured using TonoLab (Icare Finland Oy, Vantaa, Finland) under general anesthesia.

Protein/cytokine measurement and hematoxylin and eosin stain of cellular aggregates in AqH

Human AqH samples were collected at the beginning of surgeries under sterile conditions using a 27-gauge needle. A total of 100 to 200 μl of AqH were stored in silicon-coated Eppendorf tubing after centrifuging at 3000 rpm for 5 min. In mouse experiments, approximately 30 μl of AqH samples was collected using a 27-gauge needle through an oblique incision from 10 to 12 mice. AqH from mouse eyes were centrifuged at 3000 rpm for 5 min, and supernatants were diluted with distilled water up to 160 μl. Cellular aggregates were collected, and the cell smears were prepared on silane-coated slides (Muto Pure Chemicals Co., Ltd., Tokyo, Japan) using an Auto Smear CF-12C (Sakura, Tokyo, Japan) for hematoxylin and eosin stain (131-09665, Wako Pure Chemical Industries, Ltd., Osaka, Japan). For immunohistochemical evaluation in immune cells, the samples were fixed overnight in 10% neutral-buffered formalin, followed by heat-induced epitope retrieval that was performed at 121°C for 10 min in 10 mM citrate buffer (pH 6.0). Immunocytochemistry was performed with rabbit anti-MPO antibody (Dako, Glostrup, Denmark) and mouse monoclonal anti-CD10 antibody (56C6) (Nichirei, Tokyo, Japan) and visualized by Alexa Fluor 594 anti-rabbit secondary antibody (Thermo Fisher Scientific) and Alexa Fluor 488 anti-mouse secondary antibody (Thermo Fisher Scientific), respectively. Healthy and posttransplanted corneas/iris tissues of DBA2J and BALBc mice were excised on postoperative day 14 (n = 10 to 12 corneas per group). Corneas and iris tissues were washed and homogenized using a microhomogenizer (Kontes RNase-Free pellet pestle grinder, VWR, Radnor, PA, USA) in 150 μl of phosphate-buffered saline (PBS), followed by centrifugation at 15,000 rpm for 12 min at 4°C. Supernatants were diluted to 200 μl and separated into 40 μl (for protein concentration assay) and 160 μl (for cytokine assay). All samples were stored at −80°C until the measurement. Protein concentrations were measured using the DC protein assay (Bio-Rad Lab, Hercules, CA, USA). For cytokine measurement in human samples, the levels of IL-1α, IL-1β, IL-4, IL-6, IL-8, IL-10, IL-12p70, IL-13, IL-17A, IFN-α, IFN-γ, MCP-1, tumor necrosis factor–α (TNF-α), E-selectin, P-selectin, sICAM-1, macrophage inflammatory protein (MIP)–1α, MIP-1β, and IP-10 in AqH samples were measured using the Luminex (EPX200-12185-901, ProcartaPlex Human panel, Luminex, San Antonio, TX, USA) bead-based multiplex immunoassay according to previous reports without dilution (*9*). For cytokine measurement in mice, AqH samples were triplicated and the levels of IL-1β, IL-2, IL-4, IL-5, IL-6, IL-8, IL-12p70, IL-13, IL-17A, IL-18, and IFNγ. Granulocyte-macrophage colony-stimulating factor, TNF-α, MCP-1, and LIF were measured using Luminex (TFA-EPX110-20820-901 Mouse Th1/2 panel/MCP-1/LIF/IL-17A panel, Thermo Fisher Scientific). Cytokine levels in the iris and corneas were standardized using known protein concentrations.

Immunohistological evaluation

Freshly excised corneas were washed in PBS and fixated in acetone (ZO-1) or 2% formaldehyde (8-OHdG) for 15 min on ice. To block nonspecific staining, corneas were incubated in 3% normal donkey serum (S30-100ML, Chemicon, Temecula, CA, USA), 1% bovine serum albumin (A-7030, Sigma-Aldrich, St. Louis, MO, USA), and 0.3% Triton X-100 (9002-93-1, Sigma-Aldrich) for permeabilization of cell membrane (8-OHDG) for 1 hour at room temperature (RT). Corneas were then stained with conjugated anti–ZO-1 antibody (1:100; Thermo Fisher Scientific) or anti–8-OHdG antibody (1:100; JACI, Nagoya, Japan) at 4°C overnight, followed by incubation with rhodamine-conjugated secondary antibody (8-OHdG) for 30 min at RT. Each step was followed by three thorough 5-min PBS washes. For nuclei staining, corneal whole mounts were incubated with 4′,6-diamidino-2-phenylindole (0.5 μg/ml; Dojindo Laboratories, Tokyo, Japan) for 5 min at RT. Corneal whole mounts were prepared using an aqueous mounting medium containing an anti-fading agent (Fluoromount/Plus, Diagnostic BioSystems, Pleasanton, CA, USA). Specimen slides were observed under a florescence microscope (Axioplan 2 imaging, Carl Zeiss Inc., Thornwood, NY, USA).

Statistical analyses

Data were analyzed using Prism for Windows software (version 6.04, Graphpad Software Inc., San Diego, CA, USA). The D'Agostino and Pearson omnibus normality test was used to assess whether data showed a normal distribution. Spearman's correlation analyses were used to evaluate the correlations among AqH protein levels and CECD. We conducted Cox proportional hazard model using STATA/IC 14.0 for Windows (StataCorp LP, College Station, TX) to assess the clinical factors that were associated with graft failure after corneal transplantation. We selected clinical factors (preoperative AqH protein level, the presence of glaucoma, preoperative steroid use, donor/recipient age, and donor CECD) as independent variables. AqH protein levels of ≥1.0 mg/ml, the presence of glaucoma, and preoperative steroid use were dichotomized as independent variables (variance inflation factors = 1.14 to 1.16). To compare differences in protein levels across groups, unpaired Student's t test was used. Data are expressed as means ± SD. To compare differences in protein levels across groups in proteome analysis, moderated t test based on empirical Bayes approach was used (*40*). $P < 0.05$ was considered to be statistically significant. Cytokine data were also controlled with Bonferroni correction. Because there were 15 to 20 different comparisons (1 protein and 19 cytokines in human and 15 cytokines in mouse), $P < 0.0025$ (i.e., $P = 0.05/20$) was considered to be statistically significant after Bonferroni correction.

SUPPLEMENTARY MATERIALS

Supplementary material for this article is available at http://advances.sciencemag.org/cgi/content/full/6/20/eaaz5195/DC1

View/request a protocol for this paper from *Bio-protocol*.

REFERENCES AND NOTES

1. N. C. Joyce, C. C. Zhu, D. L. Harris, Relationship among oxidative stress, DNA damage, and proliferative capacity in human corneal endothelium. *Invest. Ophthalmol. Vis. Sci.* **50**, 2116–2122 (2009).
2. V. P. Hoppenreijs, E. Pels, G. F. Vrensen, J. Oosting, W. F. Treffers, Effects of human epidermal growth factor on endothelial wound healing of human corneas. *Invest. Ophthalmol. Vis. Sci.* **33**, 1946–1957 (1992).
3. K. H. Carlson, W. M. Bourne, J. W. McLaren, R. F. Brubaker, Variations in human corneal endothelial cell morphology and permeability to fluorescein with age. *Exp. Eye Res.* **47**, 27–41 (1988).
4. V. M. Ambrose, R. F. Walters, M. Batterbury, D. J. Spalton, J. I. McGill, Long-term endothelial cell loss and breakdown of the blood-aqueous barrier in cataract surgery. *J Cataract Refract Surg* **17**, 622–627 (1991).
5. D. J. Coster, M. T. Lowe, M. C. Keane, K. A. Williams; Australian Corneal Graft Registry Contributors, A comparison of lamellar and penetrating keratoplasty outcomes: A registry study. *Ophthalmology* **121**, 979–987 (2014).

6. S. V. Patel, D. O. Hodge, W. M. Bourne, Corneal endothelium and postoperative outcomes 15 years after penetrating keratoplasty. *Am. J. Ophthalmol.* **139**, 311–319 (2005).
7. N. Ishii, T. Yamaguchi, H. Yazu, Y. Satake, A. Yoshida, J. Shimazaki, Factors associated with graft survival and endothelial cell density after Descemet's stripping automated endothelial keratoplasty. *Sci. Rep.* **6**, 25276 (2016).
8. Y. Yagi-Yaguchi, T. Yamaguchi, K. Higa, T. Suzuki, N. Aketa, M. Dogru, Y. Satake, J. Shimazaki, Association between corneal endothelial cell densities and elevated cytokine levels in the aqueous humor. *Sci. Rep.* **7**, 13603 (2017).
9. H. Yazu, T. Yamaguchi, N. Aketa, K. Higa, T. Suzuki, Y. Yagi-Yaguchi, Y. Satake, T. Abe, K. Tsubota, J. Shimazaki, Preoperative aqueous cytokine levels are associated with endothelial cell loss after Descemet's stripping automated endothelial keratoplasty. *Invest. Ophthalmol. Vis. Sci.* **59**, 612–620 (2018).
10. T. Yamaguchi, K. Higa, K. Tsubota, J. Shimazaki, Elevation of preoperative recipient aqueous cytokine levels in eyes with primary graft failure after corneal transplantation. *Mol. Vis.* **24**, 613–620 (2018).
11. Y. Yagi-Yaguchi, T. Yamaguchi, K. Higa, T. Suzuki, H. Yazu, N. Aketa, Y. Satake, K. Tsubota, J. Shimazaki, Preoperative aqueous cytokine levels are associated with a rapid reduction in endothelial cells after penetrating keratoplasty. *Am. J. Ophthalmol.* **181**, 166–173 (2017).
12. O. Ibrahim, Y. Yagi-Yaguchi, K. Kakisu, J. Shimazaki, T. Yamaguchi, Association of iris damage with reduction in corneal endothelial cell density after penetrating keratoplasty. *Cornea* **38**, 268–274 (2019).
13. T. Miyai, Fuchs endothelial corneal dystrophy and mitochondria. *Cornea* **37**, S74–S77 (2018).
14. K. Jingushi, M. Uemura, N. Ohnishi, W. Nakata, K. Fujita, T. Naito, R. Fujii, N. Saichi, N. Nonomura, K. Tsujikawa, K. Ueda, Extracellular vesicles isolated from human renal cell carcinoma tissues disrupt vascular endothelial cell morphology via azurocidin. *Int. J. Cancer* **142**, 607–617 (2018).
15. M. Toda, M. Ueno, A. Hiraga, K. Asada, M. Montoya, C. Sotozono, S. Kinoshita, J. Hamuro, Production of homogeneous cultured human corneal endothelial cells indispensable for innovative cell therapy. *Invest. Ophthalmol. Vis. Sci.* **58**, 2011–2020 (2017).
16. M. O. Price, P. Calhoun, C. Kollman, F. W. Price Jr., J. H. Lass, Descemet stripping endothelial keratoplasty: Ten-year endothelial cell loss compared with penetrating keratoplasty. *Ophthalmology* **123**, 1421–1427 (2016).
17. H. M. McBride, M. Neuspiel, S. Wasiak, Mitochondria: More than just a powerhouse. *Curr. Biol.* **16**, R551–R560 (2006).
18. H. Kawashima, S. A. Prasad, D. S. Gregerson, Corneal endothelial cells inhibit T cell proliferation by blocking IL-2 production. *J. Immunol.* **153**, 1982–1989 (1994).
19. N. C. Joyce, D. L. Harris, Decreasing expression of the G1-phase inhibitors, p21Cip1 and p16INK4a, promotes division of corneal endothelial cells from older donors. *Mol. Vis.* **16**, 897–906 (2010).
20. J. Yoshino, J. A. Baur, S.-I. Imai, NAD^+ Intermediates: The biology and therapeutic potential of NMN and NR. *Cell Metab.* **27**, 513–528 (2018).
21. A. Grozio, K. F. Mills, J. Yoshino, S. Bruzzone, G. Sociali, K. Tokizane, H. C. Lei, R. Cunningham, Y. Sasaki, M. E. Migaud, S.-I. Imai, Slc12a8 is a nicotinamide mononucleotide transporter. *Nat. Metab.* **1**, 47–57 (2019).
22. Y. Motomura, H. Kitamura, A. Hijikata, Y. Matusnaga, K. Matumoto, H. Inoue, K. Araishi, S. Hori, H. Watari, J. Zhu, M. Taniguchi, M. Kubo, The transcription factor E4BP4 regulated the production of IL-10 and IL-13 in $CD4^+$ T cells. *Nat. Immunol.* **12**, 450–459 (2011).
23. B. Chang, R. S. Smith, N. L. Hawes, M. G. Anderson, A. Zaboleta, O. Savinoba, T. H. Roderick, J. R. Heckenlively, M. T. Davisson, S. W. John, Interacting loci cause severe iris atrophy and glaucoma in DBA/2J mice. *Nat. Genet.* **21**, 405–409 (1999).
24. S. Hara, M. Tsujikawa, K. Maruyama, K. Nishida, STAT3 signaling maintains homeostasis through a barrier function and cell survival in corneal endothelial cells. *Exp. Eye Res.* **179**, 132–141 (2019).
25. J. Yamada, J. W. Streilein, Induction of anterior chamber-associated immune deviation by corneal allografts placed in the anterior chamber. *Invest. Ophthalmol. Vis. Sci.* **38**, 2833–2843 (1997).
26. J.-S. Mo, M. G. Anderson, M. Gregory, R. S. Smith, O. V. Savinova, D. V. Serreze, B. R. Ksander, J. W. Streiline, S. W. M. John, By altering ocular immune privilege, bone marrow-derived cells pathogenically contribute to DBA/2J pigmentary glaucoma. *J. Exp. Med.* **197**, 1335–1344 (2003).
27. K. R. Kenyon, D. L. Van Horn, H. F. Edelhauser, Endothelial degeneration and posterior collagenous proliferation in aphakic bullous keratopathy. *Am. J. Ophthalmol.* **85**, 329–336 (1978).
28. A. Carta, V. Carelli, T. D'Adda, F. N. Ross-Cisneros, A. A. Sadun, Human extraocular muscles in mitochondrial diseases: Comparing chronic progressive external ophthalmoplegia with Leber's hereditary optic neuropathy. *Br. J. Ophthalmol.* **89**, 825–827 (2005).
29. A.-S. Benischke, S. Vasanth, T. Miyai, K. R. Katikireddy, T. White, Y. Chen, A. Halilovic, M. Price, F. Proce Jr., P. B. Liton, U. V. Jurkunas, Activation of mitophagy leads to decline in Mfn2 and loss of mitochondrial mass in Fuchs endothelial corneal dystrophy. *Sci. Rep.* **7**, 6656 (2017).
30. W. Yang, K. Nagawasa, C. Münch, Y. Xu, K. Satterstorm, S. Jeong, S. D. Hayes, M. P. Jedrychowski, F. S. Vyas, E. Zaganjor, V. Guarani, A. E. Ringel, S. P. Gygi, J. W. Harper, M. C. Haigis, Mitochondrial sirtuin network reveals dynamic SIRT3-dependent deacetylation in response to membrane depolarization. *Cell* **167**, 985–1000.e1021 (2016).
31. N. Fenouille, C. F. Bassil, I. Ben-Sahra, L. Benajiba, G. Alexe, A. Ramos, Y. Pikman, A. S. Conway, M. R. Burgess, Q. Li, F. Luciano, P. Auberger, I. Galinsky, D. J. DeAngelo, R. M. Stone, Y. Zhang, A. S. Perkins, K. Shannon, M. T. Hemann, A. Puissant, K. Stegmaier, The creatine kinase pathway is a metabolic vulnerability in EVI1-positive acute myeloid leukemia. *Nat. Med.* **23**, 301–313 (2017).
32. E. C. Genin, M. Plutino, S. Bannwarth, E. Villa, E. Cisnerros-Barroso, M. Roy, B. Ortega-Vila, K. Fragaki, F. Lespinasse, E. Pinerro-Martos, G. Augé, D. Moore, F. Burté, S. Lacas-Gervais, Y. Kageyama, K. Itoh, P. Yu-Wai-Man, H. Sesaki, J.-E. Ricci, C. Vives-Bauza, V. Paquis-Flucklinger, *CHCHD10* mutations promote loss of mitochondrial cristae junctions with impaired mitochondrial genome maintenance and inhibition of apoptosis. *EMBO Mol. Med.* **8**, 58–72 (2016).
33. R. P. Anunciado-Koza, J. Zhang, J. Ukropec, S. Bajperi, R. A. Koza, R. C. Rogers, W. T. Cefalu, R. L. Mynatt, L. P. Kozak, Inactivation of the mitochondrial carrier SLC25A25 (ATP-Mg^{2+}/P_i transporter) reduces physical endurance and metabolic efficiency in mice. *J. Biol. Chem.* **286**, 11659–11671 (2011).
34. E. Luna, E. Postol, C. Caldas, L. A. Benvenuti, J. M. Rodrigues Jr., K. Lima, J. Kalil, V. Coelho, Treatment with encapsulated Hsp60 peptide (p277) prolongs skin graft survival in a murine model of minor antigen disparity. *Scand. J. Immunol.* **66**, 62–70 (2007).
35. J. Yamada, K. Maruyama, Y. Sano, S. Kinoshita, Y. Murata, J. Hamuro, Promotion of corneal allograft survival by the induction of oxidative macrophages. *Invest. Ophthalmol. Vis. Sci.* **45**, 448–454 (2004).
36. S. K. Chauhan, U. Jurkunas, T. Funaki, M. Dastjerdi, R. Dana, Quantification of allospecific and nonspecific corneal endothelial cell damage after corneal transplantation. *Eye* **29**, 136–144 (2015).
37. D. F. LaRosa, A. H. Rahman, L. A. Turka, The innate immune system in allograft rejection and tolerance. *J. Immunol.* **178**, 7503–7509 (2007).
38. A. T. Naito, T. Sumida, S. Nomura, M.-L. Liu, T. Higo, A. Nakagawa, K. Okada, T. Sakai, A. Hashimoto, Y. Hara, I. Shimizu, W. Zhu, H. Toko, A. Katada, H. Akazawa, T. Oka, J.-K. Lee, T. Minamino, T. Nagai, K. Walsh, A. Kiuchi, M. Matsumoto, M. Botto, I. Shiojima, I. Komuro, Complement C1q activates canonical Wnt signaling and promotes aging-related phenotypes. *Cell* **149**, 1298–1313 (2012).
39. S. Shibata, Y. Murota, Y. Nishimoto, M. Yoshimura, T. Nagai, H. Okano, M. C. Siomi, Immuno-electron microscopy and electron microscopic in situ hybridization for visualizing piRNA biogenesis bodies in *Drosophila* Ovaries. *Methods Mol. Biol.* **1328**, 163–178 (2015).
40. G. K. Smyth, Linear models and empirical Bayes methods for assessing differential expression in microarray experiments. *Stat. Appl. Genet. Mol. Biol.* **3**, Article3 (2004).

Acknowledgments: We thank J. Hamuro and M. Ueno for providing the iCare equipment to measure IOP in mice and S. Yamagami for teaching us how to collect AqH in mice. We also thank Editage company for English language editing. **Funding:** This study was supported by the Grant-in-Aid for Scientific Research 15K10906 from the Ministry of Education, Culture, Sports, Science and Technology (to T.Y.), Uehara Memorial Foundation (to T.Y.), Oyama Health Foundation (to T.Y.), Takeda Science Foundation (to T.Y.), Japan Research Foundation for Clinical Pharmacology (to T.Y.), research grant from the General Insurance Association of Japan (to T.Y.), and Rohto Research Award (to T.Y.). The funding organizations had no role in the design or conduct of this research. **Author contributions:** T.Y. and K.K. contributed to the study conception and design. T.Y., K.H., Y.Y.-Y., D.T., R.Y.-M., O.I., and J.S. acquired patient samples. T.Y., D.T., and K.H. measured protein and cytokine levels in clinical/murine samples. S.S. and T.N. conducted electron microscopy. K.U. conducted the proteomic analysis. R.M. conducted the transcriptomic analysis. T.Y., O.I., and R.Y.-M. performed and analyzed the proteomic and transcriptomic data. J.Y. developed the murine model of corneal transplantation, and T.Y. performed corneal transplantations in mice. T.Y. and K.H. conducted animal experiments. T.Y. and H.N. conducted the statistical analysis. T.Y., J.Y., K.K., P.H., K.T., and J.S contributed to the analysis and interpretation of the data. T.Y. and K.K. wrote the paper. **Competing interests:** The authors declare that they have no competing interests. **Data and materials availability:** All data needed to evaluate the conclusions in the paper are present in the paper and/or the Supplementary Materials. Additional data related to this paper may be requested from the authors.

Submitted 16 September 2019
Accepted 28 February 2020
Published 13 May 2020
10.1126/sciadv.aaz5195

Citation: T. Yamaguchi, K. Higa, Y. Yagi-Yaguchi, K. Ueda, H. Noma, S. Shibata, T. Nagai, D. Tomida, R. Yasu-Mimura, O. Ibrahim, R. Matoba, K. Tsubota, P. Hamrah, J. Yamada, K. Kanekura, J. Shimazaki, Pathological processes in aqueous humor due to iris atrophy predispose to early corneal graft failure in humans and mice. *Sci. Adv.* **6**, eaaz5195 (2020).

Science Advances

Pathological processes in aqueous humor due to iris atrophy predispose to early corneal graft failure in humans and mice

Takefumi Yamaguchi, Kazunari Higa, Yukari Yagi-Yaguchi, Koji Ueda, Hisashi Noma, Shinsuke Shibata, Toshihiro Nagai, Daisuke Tomida, Ririko Yasu-Mimura, Osama Ibrahim, Ryo Matoba, Kazuo Tsubota, Pedram Hamrah, Jun Yamada, Kohsuke Kanekura and Jun Shimazaki

Sci Adv **6** (20), eaaz5195.
DOI: 10.1126/sciadv.aaz5195

Science Advances (ISSN 2375-2548) is published by the American Association for the Advancement of Science, 1200 New York Avenue NW, Washington, DC 20005. The title *Science Advances* is a registered trademark of AAAS.